




Collective Slip Results on Mhd Unstable Flow on Porous Stretching Sheet

Venkata Chandra Sekhar Kasulanati 

Department of Mathematics, College of Engineering, Koneru Lakshmaiah Education Foundation Vaddeswaram, Guntur 522302, India

Corresponding Author Email: kasulanati22@rediffmail.com

Copyright: ©2024 The authors. This article is published by IETA and is licensed under the CC BY 4.0 license (<http://creativecommons.org/licenses/by/4.0/>).

<https://doi.org/10.18280/ijht.420132>

ABSTRACT

Received: 21 September 2023

Revised: 25 December 2023

Accepted: 15 January 2024

Available online: 29 February 2024

Keywords:

slip effects, MHD, unsteady, porous, stretching sheet

The present work presents a numerical investigation of the combined sliding outcomes of the MHD unstable heat and mass transport phenomena of the Casson fluid above the stretched sheet. The stretched sheet moving at a non-uniform velocity and the magnetic field were taken into consideration. We reconstruct the flow-related equations as linked non-linear partial differential equations by using similarity transformations. The main conclusions drawn from this work indicate that flow velocity decreases with increasing porosity levels and the Casson parameter. On the other hand, a rise in the Dufour number increases the fluid velocity. The impact of various physical parameters on the flow field is graphically depicted with the help of the MATLAB application BVP4C.

1. INTRODUCTION

Hydromagnetic flow has many uses in industry, physics, and engineering domains, including bioengineering; nevertheless, studying hydromagnetic flow over surfaces that are either expanding or contracting is a difficult task. Magnetic fields significantly impact the flow of electrically conducting viscous fluids in applications like glass, paper, crude oil refining, and magnetic materials. Several researchers have explored mathematical solutions using a no-slip boundary condition to study flow phenomena. The relative velocity of a (Newtonian) fluid with respect to any solid surface is zero, which is the principle underlying the no-slip condition. Nevertheless, there are scenarios where this assumption is not valid. In this paper, we explore the implications of slip at the wall on fluid flow. The slip condition suggests that fluid particles at the solid boundary do not adhere to or stick to the surface instead, they undergo some form of slip or relative motion with respect to the solid. The study of vibrating valves has been stimulated by the significance of slip boundary conditions in microchannels and nanochannels can take place in fluids containing concentrated suspensions. Soltani and Yilmazor [1] studied the rheological behavior of concentrated suspensions with a Newtonian matrix, aluminum powder, and glass beads, focusing on wall slip using a parallel disk rheometer. Impure fluids such as mixtures and spray solutions can exhibit incomplete velocity slip. In addition to this at borderline of pipes, walls and embowed surfaces slip effects can be seen. The utilization of the Navier slip velocity condition is a prevalent method in the investigation of slip phenomena. Different authors, like Mahanthesh et al. [2], Hayat et al. [3], Motsa and Shateyi [4] gone through slip effects for different flow phenomenas. Shateyi and Mabood [5] extended the work of slide effects on MHD flows. The

applications of magnetohydrodynamic fluid flows on a stretching sheet are significant in engineering and industry, underlining their importance [6]. Magnetohydrodynamic (MHD) flow can be applied in a variety of situations, such as thermionic freezing, vessels, heat neutralization and alloy removal, liquid alloy fuel containers, nuclear power plants, and nuclear activities. Mabood et al. [7] investigated the influence of thermal inputs and chemical reactions on the behavior of rotating magnetohydrodynamic fluids. The effect of erosion warming on MHD ferro-fluid with heat emission was investigated by Kumar et al. [8]. Abbas et al. [9], Makinde et al. [10], and Ibrahim et al. [11] performed a computational investigation to examine the impact of radiation on magnetohydrodynamic (MHD) nanofluids with chemical reactions. Prasannakumara et al. [12] conducted a study investigating the impact of numerous slides and thermal emissions on the stable flow, as well as the heat and mass transport of a condensed Jeffrey nanofluid when it interacts with a parallel dilatant surface. Apart from these studies many researchers have done significant work in connection with the above work [13-22]. Mabood and Shateyi [23] extended the work to the multiple slips for MHD flows in permeable frame of reference including Soret effect. One of the main issues in fluid dynamics is analyzing the flow and heat transfer of a viscous fluid across a stretched sheet. The study of chemical and metallurgical engineering fields can also benefit from knowledge of Casson fluid flow over a stretched sheet. The study focuses on the mass and heat transfer of Casson fluid flow across a stretched surface, despite its significant non-Newtonian behavior in technology and industry. This extends the work of Mabood and Shateyi [23] to include MHD Casson fluid flow, taking into account the permeability parameter and the Dufour effect.

2. FORMULATION OF THE PHENOMENA

An incompressible two-dimensional MHD electronically controlling fluid flow across a porous stretched surface is studied in the context of thermal emission. As shown in Figure 1, the horizontal and vertical directions are represented by the x- and y-axes, respectively, in a two-dimensional coordinate system. A thin sheet that is positioned and completely aligned with the x-axis is metaphorically compared to a metal plate, as shown. Along the x-axis, the sheet is moving continuously in the positive x-direction at a variable speed while meeting the criteria $\lambda t < 1$ for a positive constant and stretching rate. The magnetic field, the magnetic field, denoted by the letter "x", is a coordinate that changes with distance from the origin over the surface. The magnetic field energy is denoted by B_0 . It is anticipated that the induced magnetic field will be significantly smaller than the applied magnetic field since it is constrained by the charge's velocity. The equations that explain the flow are as follows:

$$\left(\frac{\partial u}{\partial x}\right) + \left(\frac{\partial v}{\partial y}\right) = 0 \quad (1)$$

$$\frac{\partial u}{\partial t} + u\left(\frac{\partial u}{\partial x}\right) + v\left(\frac{\partial u}{\partial y}\right) = v\left(1 + \frac{1}{\beta}\right)\frac{\partial^2 u}{\partial y^2} - \frac{\sigma B(x)^2 u}{\rho} - (T_\infty - T)g\beta_T - (C_\infty - C)g\beta_C - \frac{vu}{k_1}, \quad (2)$$

$$\frac{\partial T}{\partial t} + u\left(\frac{\partial T}{\partial x}\right) + v\left(\frac{\partial T}{\partial y}\right) = \alpha\left(1 + \frac{16T_\infty^3\sigma^*}{3k^*\kappa}\right)\frac{\partial^2 T}{\partial y^2} + Du\frac{\partial^2 C}{\partial y^2}, \quad (3)$$

$$\frac{\partial C}{\partial t} + u\left(\frac{\partial C}{\partial x}\right)^{-1} + v\left(\frac{\partial C}{\partial y}\right)^{-1} = D_M\frac{\partial^2 C}{\partial y^2}. \quad (4)$$

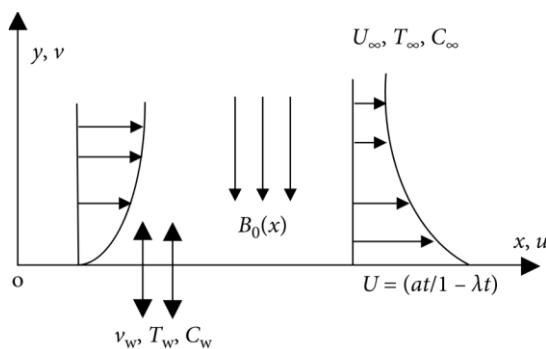


Figure 1. Configuration and coordinate system

The preceding description provides an overview of the model's boundary conditions.

$$u = U(x, t) + U_s, T = T_\infty + T_0\left(\frac{ax}{2v(1-\lambda t)^2}\right) + T_s, \quad (5)$$

$$C = C_\infty + C_0\left(\frac{2v(1-\lambda t)^2}{ax}\right)^{-1} + C_s, \quad \text{at } y=0$$

$$u \rightarrow 0, T - T_\infty \rightarrow 0, C - C_\infty \rightarrow 0,$$

as $y \rightarrow \infty$

as such $0 \leq T_0 \leq T_w$ and $0 \leq C_0 \leq C_w$ are applicable if $(1-\lambda t) > 0$. Eq. (1) is fulfilled by defining the stream functions $u = \left(\frac{\partial \psi}{\partial x}\right), v = \left(\frac{\partial \psi}{\partial y}\right)$.

Let's introduce the following dimensionless functions:

$$\eta = \sqrt{\frac{a}{v(1-\lambda t)}}y, \quad \psi = \sqrt{\left(\frac{(1-\lambda t)}{av}\right)^{-1}}xf(\eta)$$

$$C = C_\infty + C_0\left(\frac{ax}{2v(1-\lambda t)^2}\right)\phi(\eta). \quad (6)$$

$$T = T + T_0\left(\frac{ax}{2v(1-\lambda t)^2}\right)\theta(\eta),$$

Replacing Eq. (6) into (2), (3) and (4) we get the following.

$$\left(1 + \frac{1}{\beta}\right) f'''(\eta) + f(\eta)f''(\eta) - f'(\eta)^2 - \delta\left(\frac{\eta}{2}f''(\eta) + f'(\eta)\right) - (M^2 + k)f(\eta) + \frac{Gr}{2}\theta(\eta) + \frac{Gc}{2}f(\eta) = 0, \quad (7)$$

$$\frac{1+R}{Pr}\theta''(\eta) + Du f''(\eta) + f(\eta)\theta'(\eta) - f'(\eta)\theta(\eta) - \frac{\lambda}{2a}\eta\theta'(\eta) - \frac{2\lambda}{a}\theta(\eta) = 0, \quad (8)$$

$$\phi''(\eta) + Sc(\phi(\eta)\phi'(\eta) - \phi'(\eta)\phi(\eta)) - Sc\delta\left(2\phi(\eta) + \frac{\eta}{2}\phi'(\eta)\right) = 0. \quad (9)$$

The transmuted extremity positions regarding the phenomena are:

$$f_w = f(0), \frac{f'(0)-1}{s_f} = f''(0), \frac{\theta(0)-1}{s_\theta} = \theta'(0)$$

$$\frac{\phi(0)-1}{s_f} = \phi'(0) \quad (10)$$

$$f'(\eta) \rightarrow 0, \theta(\eta) \rightarrow 0, \phi(\eta) \rightarrow 0 \text{ as } \eta \rightarrow \infty,$$

where,

$$\delta = \frac{\lambda}{a}, Gr = \frac{g\beta_T T_0}{av}, Gc = \frac{g\beta_C C_0}{av}, Pr = \frac{\nu}{\alpha}, R = \frac{16T_\infty^3\sigma^*}{3k^*\kappa},$$

$$M = \sqrt{\frac{\sigma}{\rho a}}B_0, Sc = \frac{\nu}{D_M}, Du = \frac{D_M C_0}{vT_0}.$$

The local skin resistance coefficient S_f , local Nusselt number Nu , and local Sherwood number Sh are among the engineering-relevant physical characteristics, and they are described as:

$$S_f = \frac{\mu}{\rho U_w^2} \left(\frac{\partial u}{\partial y} \right)_{y=0} \quad (11)$$

$$Nu = \frac{x}{\kappa(T_w - T_y)} \left[\kappa \left(\frac{\partial T}{\partial y} \right)_{y=0} - \frac{4\sigma^*}{3k^*} \left(\frac{\partial T^4}{\partial y} \right)_{y=0} \right], \quad (12)$$

$$Sh = - \frac{x}{(C_w - C_\infty)} \left(\frac{\partial C}{\partial y} \right)_{y=0} \quad (13)$$

By substituting Eq. (6) into (11) to (13) we can obtain the dimensionless form of equations

$$S_{fr} = \sqrt{Re_x} S_f, \quad Nu_r = \frac{Nu}{\sqrt{Re_x}} = -[1+R]\theta'(0), \quad Sh_r = \frac{Sh}{\sqrt{Re_x}} = -f'(0),$$

Here, Re_x is the local Reynolds number, defined as $\frac{U_w x}{\nu}$. Sh_r , Nu_r and S_{fr} symbolizes the decreased Sherwood number, the decreased Nusselt number, and the decreased skin friction.

3. METHOD OF SOLUTION

The transformed ordinary differential equation (ODE) and its corresponding boundary conditions were numerically solved using the MATLAB tool BVP4C. This method provides a solution that is continuous on the specified interval $[a, b]$ and has a continuous first derivative there. BVP4C effectively addresses a system of algebraic equations to determine the numerical solution for a boundary value problem (BVP) at each mesh point.

The `bvp4c` function integrates a system of differential equations, taking into consideration the initial solution guess provided by `Solinit` and the boundary conditions specified by `bcfun`. The `bvpinit` function provides the initial estimate and specifies the locations where the boundary conditions are applied.

The approach used to solve the coupled nonlinear ODEs (Eqs. (7), (8), and (9)) is detailed below.

1. Define Variables.
2. Construct the collection of Ordinary Differential Equations (ODEs).
3. Define the boundaries utilizing the variables that have been established.
4. Define the ODE Function.
5. Establish the Boundary Condition (BC) function, specifying conditions for the problem.
6. Set Up the Boundary Value Problem (BVP).
7. Solve the BVP.

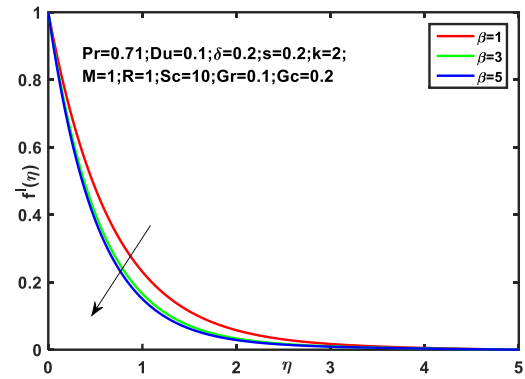
The dissimilar critical variables were investigated for their influence on the displacement rate, temperature, and concentration.

The step size and concurrence bench mark were considered as $\Delta\eta=0.001$. The asymptotic conditions at the boundary as per Eq. (10) were estimated by fixing the similarity variable η_{max} to 5, as follows:

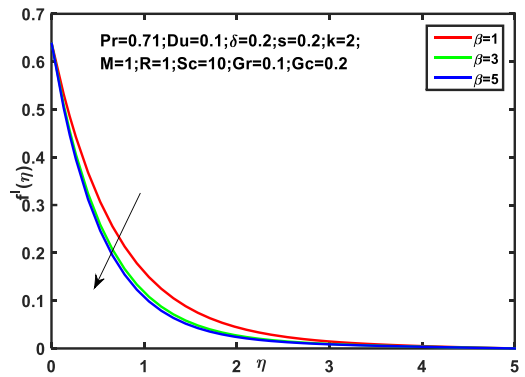
$$Max \eta = 5, \quad f'(5) = \theta(5) = \varphi(5) = 0.$$

4. DISCUSSION ON OUTCOMES

In order to enhance comprehension of the issue, Figures 2(a) and (b) with and without slip present graphical representations of the impacts of many factors on temperature, velocity, and concentration. As viscosity increases, flow momentum decreases, raising the Casson variable β and subsequently lowering the flow's velocity. This is seen in Figures 2(a) and 2(b).



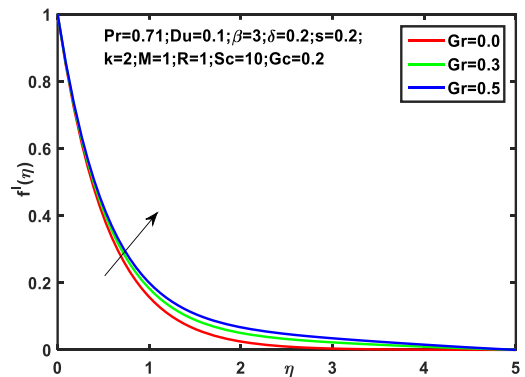
(a) Control of Casson variable on displacement Rate without slip



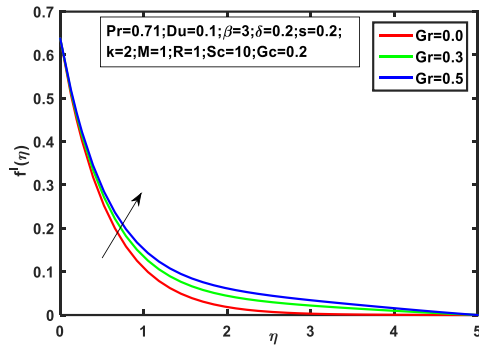
(b). Control of Casson variable on displacement Rate with slip

Figures 2. Control of Casson variable on displacement rate

The differences in velocity profiles for various thermal Grashof number values, Gr , are shown in Figures 3(a) and 3(b). It may be described as the thermal buoyant force divided by the viscous hydrodynamic force. Impact of this force is fruitful to a greater extent in the alliance of free convection, which rises momentum rate of the flow.



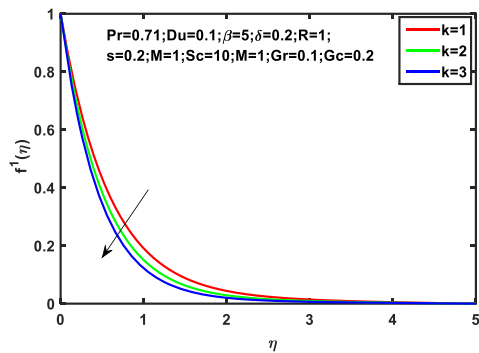
(a) Displacement rate with respect to solutal Grashof number on velocity profiles without slip



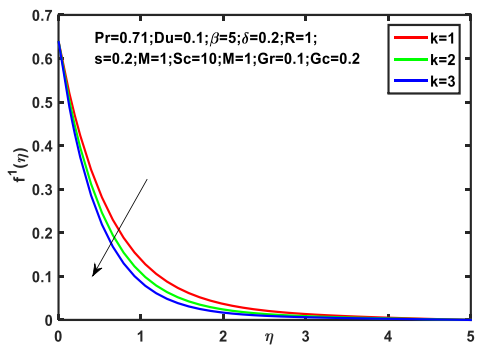
(b) Displacement rate with respect to solutal Grashof number on velocity distributions with slip

Figure 3. Displacement rate with respect to solutal Grashof number

The portrayal of displacement rate has been represented in Figures 4(a) and 4(b). As porosity (k) increases while keeping other parameters constant, the velocity and density at the borderline also increase. The permeable medium becomes less favorable, resulting in a decrease in flow velocity.

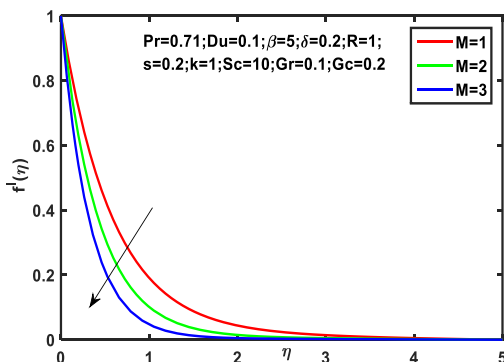


(a) Porosity's effect on non-slip velocity profiles

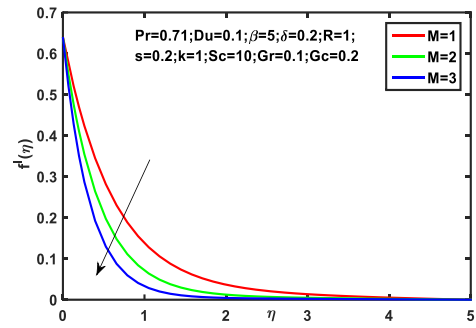


(b) Porosity's effect on velocity profiles with slip

Figure 4. Porosity's effect on non-slip velocity profiles



(a) Magnetic parameter control on slippage-free displacement profiles

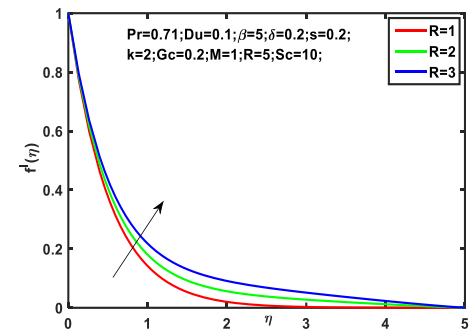


(b) Controlling the magnetic parameter on displacement patterns that involve slip

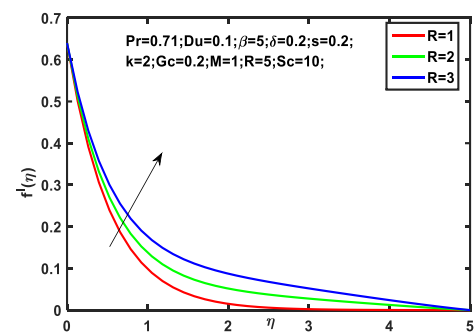
Figure 5. Magnetic parameter control on displacement profiles

By interacting with the magnetic field, the generated currents produce the immune force, an opposing force that lowers velocity. The acceleration of the flow decreases as the magnetic variable increases, as shown in Figures 5(a) and 5(b).

The effects of the radiation variable are shown in Figures 6(a) and 6(b). The displacement rate of the flow increases as the heat emission parameter increases. This is because the density of the thermal boundary layer increases with an increased radiation parameter.



(a) Impact of the heat emission parameter on velocity profiles in the absence of slip

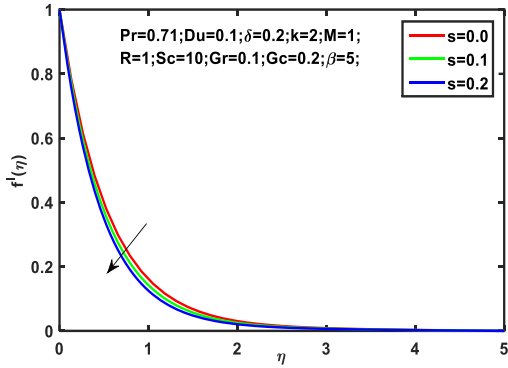


(b) Consequence of heat emission parameter on velocity distributions with slip

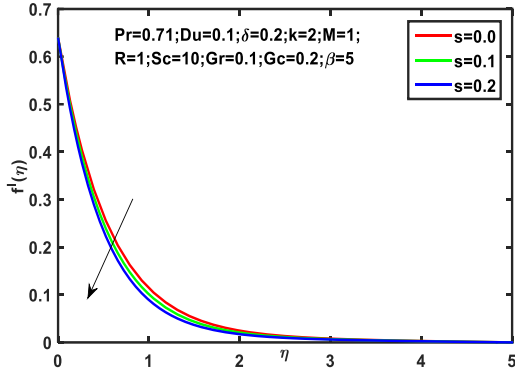
Figure 6. Consequence of heat emission parameter on velocity distributions

Figures 7(a) and 7(b) show that, when suction is increased, the fluid flow velocity decreases due to decreased diffusion and a thinner fluid layer at the surface. The Prandtl number, or the ratio of fluid flow ease to heat conduction ease, is responsible for much of this occurrence.

Figures 8(a) and 8(b) demonstrate how the flow temperature rises as the heat emission parameter increases. The increase in heat emission parameter is attributed to the growth in thermal boundary layer density.

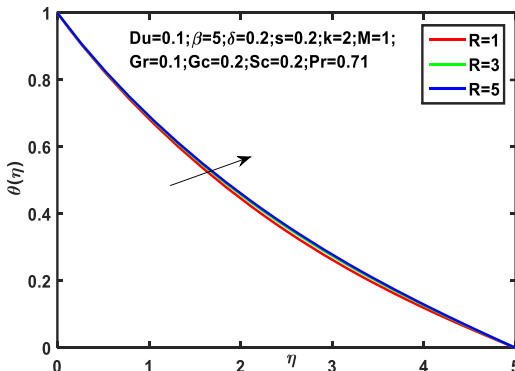


(a) Performance of different suction parameter levels without any slippage

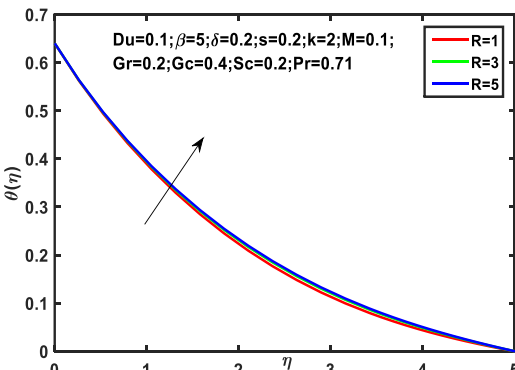


(b) Speed profile for different suction parameter values with slip

Figure 7. Performance of different suction parameter levels on velocity profiles

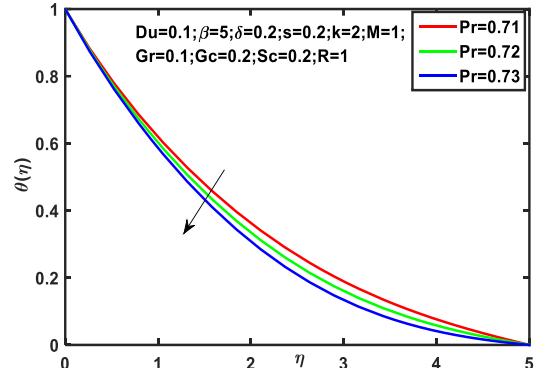


(a) Temperature profiles in the presence of slip, specifically examining the emission parameter

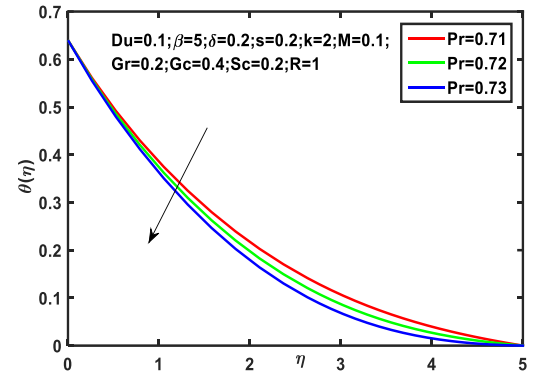


(b) Temperature profiles in the presence of slip, specifically examining the emission parameter

Figure 8. Differences in temperature profiles for various heat emission parameter values

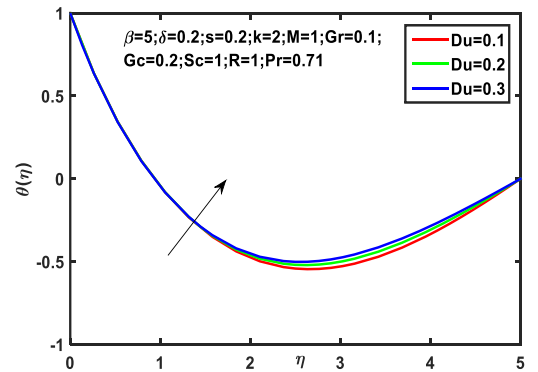


(a) Temperature profiles in the absence of slip, specifically examining the Prandtl number

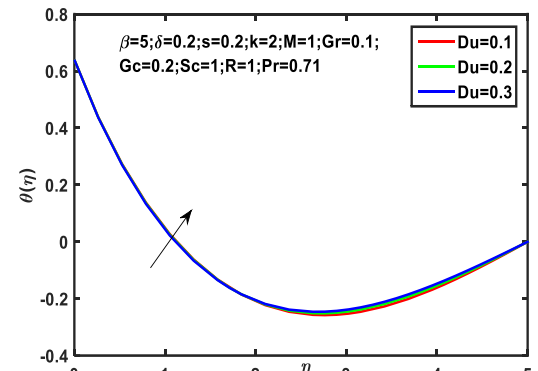


(b) Temperature profiles in the presence of slip, specifically examining the Prandtl number

Figure 9. Temperature profiles specifically under the influence of Prandtl number



(a) Result of Dufour variable on thermal profiles with slip



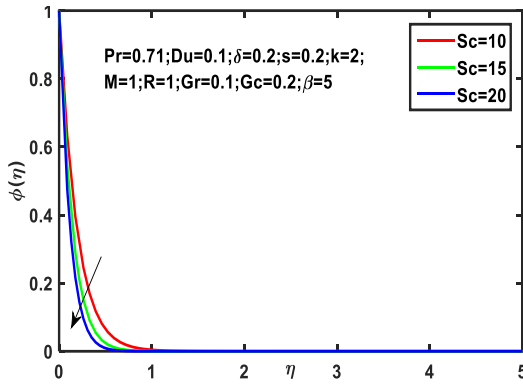
(b) Result of Dufour variable on thermal profiles with slip

Figure 10. Result of Dufour variable on thermal profiles

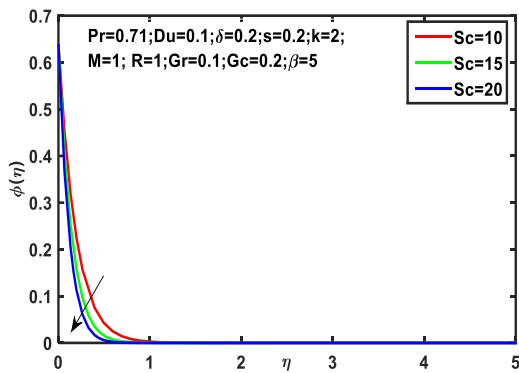
Heat conductivity and Prandtl number have an inverse relationship, as seen in Figures 9(a) and 9(b). This relationship is observed as a decrease in the boundary layer temperature as the Prandtl number grows.

As the Dufour number rises, so does the fluid's temperature. This is seen in Figures 10(a) and 10(b).

Figures 11(a) and 11(b) show how the Schmidt number affects concentration profiles. The mixture diffusivity reduces with increasing Schmidt number, facilitating a more even distribution of the solutal effect. Consequently, the concentration drops more gradually.



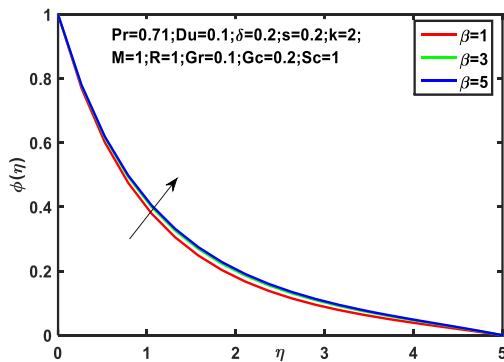
(a) Results of concentration with reference to Schmidt number without slip



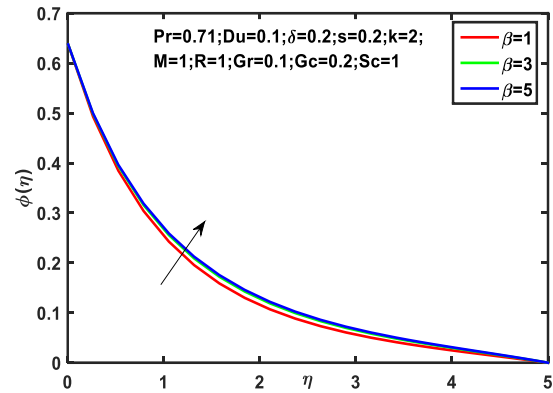
(b) Results of concentration with reference to Schmidt number with slip

Figure 11. Results of concentration with reference to Schmidt number

A fluid with a high viscosity and an increase in congregation is produced by increasing the Casson parameter. Figures 12(a) and 12(b) depict this.



(a) Impression of Casson parameter on concentration profiles without slip



(b) Impression of Casson parameter on concentration profiles with slip

Figure 12. Impression of Casson parameter on concentration profiles

A comparison analysis was conducted for the friction coefficient $-f''(0)$ at the surface and the rate of heat transfer $-\theta'(0)$ in order to verify the present findings and evaluate the accuracy of the continuing analysis.

Table 1 shows that increasing the stretching parameter increases the amount of skin friction.

Table 1. Comparing different values of δ when $f_w=M=Gr=Gc=S_f=0$

δ	Fazle Mabood and Stanford Shateyi	Present Results
0.8	1.2615	1.2619
1.2	1.3780	1.3782

Table 2 illustrates how the skin friction coefficient varies in the absence of suction in accordance with the findings of [21], extending slip parameters as the magnetic variable M rises. We can observe that due to rise in magnetic parameter skin friction enlarges significantly owing to Lorentz forces generated by electromagnetic forces.

Table 2. Examination of $-f''(0)$ different values of M when $f_w=\delta=S_f=0$

M	Fazle Mabood and Stanford Shateyi	Present Results
0	-1.0000	-1.0014
1	1.4142	1.4142
5	2.4494	2.4653
10	3.3166	3.3182
50	7.1414	7.1428
100	10.0498	10.0408
500	22.3830	22.3800

Table 3 displays a comparison between the present heat transfer rate numbers and those from [23]. It has been demonstrated that the Prandtl number has a significant impact on the heat transfer rate. As the Prandtl number rises, so does the rate of heat transport.

Table 3. Distinguishing of heat exchange rate $-\theta'(0)$ when $M=f_w=S_f=S_\theta=\delta=Gr=Gc=R=0$

Pr	Fazle Mabood and Stanford Shateyi	Present Results
0.72	0.8088	0.8095
1	1.0000	1.0012
3	1.9237	1.9229
10	3.7207	3.7306

5. CONCLUSIONS

The current article undertakes an in-depth analysis of collective slip effects in the context of unstable Casson fluid flow. To translate the partial differential equations regulating these occurrences into conventional ones, appropriate similarity transformations are provided. The MATLAB tool BVP4C was used to determine the problem's numerical solution. This work extends the work of Mabood and Shateyi [23] by methodically examining mass and heat transport in Casson fluid flow over extended surfaces. We reach the following important results by means of the graphical narration of several physical parameter impacts:

- 1) As suction, permeability, magnetic field, and Casson parameters increase, the fluid velocity falls.
- 2) The fluid velocity increased as the radiation parameter and thermal gradient number increased.
- 3) While rising radiation parameter and Dufur number values raise fluid temperature, rising Prndtl number values decelerate the fluid's temperature.
- 4) Increasing values of Casson parameter gives increment in fluid concentration and increasing in Schmidt number decreases fluid concentration.
- 5) The above results were depicted through graphs separately for fluid flow without slip and with slip.
- 6) Existing results of heat exchange and skin friction are compared with the values obtained in the present work with help of the tables.
- 7) In general, the conclusions drawn from this study have the potential to yield advantages across diverse sectors, including industrial processes, and can be valuable for professionals in engineering, physics, and mathematics.

The current methodology has applications in biomedical engineering, namely in examining blood flow properties as a Casson fluid across an elongating arterial wall.

REFERENCES

- [1] Soltani, F., Yilmazer, L. (1998). Slip velocity and slip layer thickness in flow of concentrated suspensions. *Journal of Applied Polymer Science*, 70(3): 515-522.
- [2] Mahanthesh, B., Mabood, F., Gireesha, B.J., Gorla, R.S.R. (2017). Effects of chemical reaction and partial slip on the three-dimensional flow of a nanofluid impinging on an exponentially stretching surface. *European Physical Journal Plus*, 132(3): 1-18. <https://doi.org/10.1140/epjp/i2017-11389-8>
- [3] Hayat, T., Hina, S., Ali, N. (2010). Simultaneous effects of slip and heat transfer on the peristaltic flow. *Communications in Nonlinear Science and Numerical Simulation*, 15(6): 1526-1537. <https://doi.org/10.1016/j.cnsns.2009.06.032>
- [4] Motsa, S.S., Shateyi, S. (2012). Successive linearization analysis of the effects of partial slip, thermal diffusion, and diffusion thermo on steady MHD convective flow due to a rotating disk. *Mathematical Problems in Engineering*, 2012, Article ID 397637. <https://doi.org/10.1155/2012/397637>
- [5] Shateyi, S., Mabood, F. (2017). MHD mixed convection slip flow near a stagnation-point on a non-linearly vertical stretching sheet in the presence of viscous dissipation. *Thermal Science*, 21(6): 2731-2745. <https://doi.org/10.2298/TSCI151025219S>
- [6] Mabood, F., Das, K. (2016). Melting heat transfer on hydromagnetic flow of a nanofluid over a stretching sheet with radiation and second-order slip. *European Physical Journal Plus*, 131(1): 1-12. <https://doi.org/10.1140/epjp/i2016-16003-1>
- [7] Mabood, F., Ibrahim, S.M., Lorenzini, G. (2017). Chemical reaction effects on MHD rotating fluid over a vertical plate embedded in porous medium with heat source. *Journal of Engineering Thermophysics*, 26(3): 399-415. <https://doi.org/10.1134/S1810232817030109>
- [8] Kumar, K.A., Ramana Reddy, J.V., Sugunamma, V., Sandeep, N. (2017). Impact of frictional heating on MHD radiative ferrofluid past a convective shrinking surface. *Defect and Diffusion Forum*, 378: 157-174. <https://doi.org/10.4028/www.scientific.net/DDF.378.157>
- [9] Abbas, Z., Wang, Y., Hayat, T., Oberlack, M. (2009). Slip effects and heat transfer analysis in a viscous fluid over an oscillatory stretching surface. *International Journal for Numerical Methods in Fluids*, 59(4): 443-458. <https://doi.org/10.1002/flid.1825>
- [10] Makinde, O.D., Mabood, F., Ibrahim, M. (2018). Chemically reacting on MHD boundary-layer flow of nanofluids over a nonlinear stretching sheet with heat source/sink and thermal radiation. *Thermal Science*, 22(1): 495-506. <https://doi.org/10.2298/TSCI151003284M>
- [11] Ibrahim, S.M., Kumar, P.V., Lorenzini, G., Lorenzini, E., Mabood, F. (2017). Numerical study of the onset of chemical reaction and heat source on dissipative MHD stagnation point flow of Casson nanofluid over a nonlinear stretching sheet with velocity slip and convective boundary conditions. *Journal of Engineering Thermophysics*, 26(2): 256-271. <https://doi.org/10.1134/S1810232817020096>
- [12] Prasannakumara, B.C., Krishnamurthy, M.R., Gireesha, B.J., Gorla, R.S.R. (2016). Effect of multiple slips and thermal radiation on MHD flow of Jeffery nanofluid with heat transfer. *Journal of Nanofluids*, 5(1): 82-93. <https://doi.org/10.1166/jon.2016.1198>
- [13] Chamkha, A.J., Aly, A.M., Mansour, M.A. (2010). Similarity solution for unsteady heat and mass transfer from a stretching surface embedded in a porous medium with suction/injection and chemical reaction effects. *Chemical Engineering Communications*, 197(6): 846-858. <https://doi.org/10.1080/00986440903359087>
- [14] Ali, M.E. (1994). Heat transfer characteristics of a continuous stretching surface. *Wärme-und Stoffübertragung*, 29(4): 227-234. <https://doi.org/10.1115/1.3247387>
- [15] Ibrahim, S.M., Mabood, F., Kumar, P.V., Lorenzini, G., Lorenzini, E. (2018). Cattaneo-Christov heat flux on UCM flow across a melting surface with cross diffusion and double stratification. *Italian Journal of Engineering Science Tecnica Italiana*, 62(1): 7-16. <http://doi.org/10.18280/ijes.620102>
- [16] Shateyi, S., Mabood, F., Lorenzini, G. (2017). Casson fluid flow free convective heat and mass transfer over an unsteady permeable stretching surface considering viscous dissipation. *Journal of Engineering Thermophysics*, 26(1): 39-52. <http://doi.org/10.1134/S1810232817010052>
- [17] Mabood, F., Shafiq, A., Hayat, T., Abelman, S. (2017).

- Radiation effects on stagnation point flow with melting heat transfer and second order slip. *Results in Physics*, 7: 31-42. <https://doi.org/10.1016/j.rinp.2016.11.051>
- [18] Mabood, F., Ibrahim, S., Lorenzini, G., Lorenzin, E. (2017). Radiation effects on Williamson nanofluid flow over a heated surface with magnetohydrodynamics. *International Journal of Heat and Technology*, 35(1): 196-204. <http://doi.org/10.18280/ijht.350126>
- [19] Inouye, K., Tate, A. (1974). Finite difference version of quasilinearization applied to boundary layer equations. *AIAA Journal*, 12(1): 558-560. <https://doi.org/10.2514/3.49286>
- [20] Bellman, R.E., Kalaba, R.E. (1965). *Quasilinearization and Non-Linear Boundary Value Problems*. America Elsevier. <https://doi.org/10.4236/am.2011.28136>
- [21] Khan, S.A., Nie, Y., Ali, B. (2020). Multiple slip effects on MHD unsteady viscoelastic nano-fluid flow over a permeable stretching sheet with radiation using the finite element method. *SN Applied Sciences*, 2: 1-14. <https://doi.org/10.1007/s42452-019-1831-3>
- [22] Seid, E., Haile, E., Walelign, T. (2022). Multiple slip, Soret and Dufour effects in fluid flow near a vertical stretching sheet in presence magnetic nanoparticles. *International Journal Thermo Fluids*, 13: 1-10. <https://doi.org/10.1016/j.ijft.2022.100136>
- [23] Mabood, F., Shateyi, S. (2019). Multiple slip effects on MHD unsteady flow heat and mass transfer impinging on permeable stretching sheet with radiation. *Hindawi Modelling and Simulation in Engineering*, 2019, Article ID 3052790. <https://doi.org/10.1155/2019/3052790>